Earth and Planetary Science Letters 389 (2014) 95–104

Contents lists available at ScienceDirect

Earth and Planetary Science Letters

www.elsevier.com/locate/epsl

Pyrite multiple-sulfur isotope evidence for rapid expansion and contraction of the early Paleoproterozoic seawater sulfate reservoir

Clint Scott [a,*,1], Boswell A. Wing [a], Andrey Bekker [b,c], Noah J. Planavsky [c], Pavel Medvedev [d], Steven M. Bates [c], Misuk Yun [b], Timothy W. Lyons [c]

[a] Department of Earth and Planetary Sciences and GEOTOP, McGill University, Montreal, Quebec, Canada
[b] Department of Geological Sciences, University of Manitoba, Winnipeg, Manitoba, Canada
[c] Department of Earth Sciences, University of California, Riverside, CA, USA
[d] Institute of Geology, Karelian Research Center, RAS, Petrozavodsk, Russia

ARTICLE INFO

Article history:
Received 28 December 2012
Received in revised form 25 November 2013
Accepted 6 December 2013
Available online xxxx
Editor: G.M. Henderson

Keywords:
Precambrian
seawater sulfate
sulfur isotopes
black shales

ABSTRACT

Earth's oxygenation is often described in terms of two unidirectional steps at the beginning and end of the Proterozoic Eon, separated by a long-lived intermediate redox state. Recent work defines a more complicated path to oxygenation, exemplified by an apparent drop in oxidation state following the early Paleoproterozoic Lomagundi carbon isotope excursion. The timing of this proposed drop in oxidation state is not well constrained, and it is not clear how it relates to redox conditions during the remainder of the Proterozoic. Here we present a study of pyrite multiple-sulfur isotopes, supported by Fe speciation and organic carbon isotopes, from early Paleoproterozoic black shales. We find evidence for the rapid expansion of the seawater sulfate reservoir during the Great Oxidation Event at ca. 2.3 Ga followed by a subsequent contraction in the size of the seawater sulfate reservoir at ca. 2.05 Ga. This scenario is consistent with the emerging view of a rise and fall in surface oxidation state during the early Paleoproterozoic. Comparison of our new data to other records of the seawater sulfate reservoir suggests that the elevated sulfate concentrations that characterize the early Paleoproterozoic did not return until the late Neoproterozoic.

Published by Elsevier B.V.

1. Introduction

The oxygenation of Earth's atmosphere and oceans is a major focus of Precambrian biogeochemistry. Early models for Earth's oxygenation called upon two unidirectional steps at the beginning and end of the Proterozoic eon. It is generally agreed upon that permanent atmospheric oxygenation (a switch to $>10^{-5}$ present atmospheric levels (PAL); Pavlov and Kasting, 2002) occurred between 2.47 and 2.32 Ga (Holland, 2002; Bekker et al., 2004) during the onset of the so-called 'Great Oxidation Event' [GOE]. A second step in surface oxygenation likely occurred in the late Neoproterozoic (Scott et al., 2008; Sahoo et al., 2012). Because this second oxygenation event is roughly coincident with the first appearance of macroscopic metazoans in the rock record, a causal relationship is commonly evoked. Given the likelihood of Neoproterozoic deep-water oxygenation (Canfield, 2005), estimates for atmospheric oxygen in the immediate aftermath of this second oxygenation event are at minimum between 40%–60% PAL (e.g., Canfield, 1998; Ozaki and Tajika, 2013). In between these two steps Earth is believed to have experienced a long-lived intermediate state, more oxidized than the Archean (Canfield, 1998; Scott et al., 2008), but insufficiently oxygenated to allow for the evolution of animals (Narbonne, 2005).

Emerging work describes a more complicated picture of oxygenation, particularly in the Paleoproterozoic era, and it is increasingly clear that oxygenation did not occur as a single, unidirectional step (Canfield, 2005; Frei et al., 2009; Bekker and Holland, 2012; Planavsky et al., 2012; Partin et al., 2013). This new scenario raises a number of important questions. First, what was the magnitude and duration of the GOE? Goldblatt et al. (2006) predicted an abrupt transition from oxygen-free to oxygen-rich conditions across the GOE, and Planavsky et al. (2012) provided evidence for sulfate-rich oceans during the GOE and a contraction of the seawater sulfate reservoir (SSR) following the Lomagundi carbon isotope excursion. Conversely, Kump et al. (2011) argued for a progressive oxygenation that culminated before 2.05 Ga. Second, when did the surface oxidation state rebound and to what degree? Canfield (2005) and Frei et al. (2009) argued for a gradual drop in surface oxidation state prior to the return of iron formations at ca. 1.9 Ga but implied that Earth's surface oxidation state soon returned to early Paleoproterozoic levels. Finally, does the emerging picture of

* Corresponding author.
E-mail address: clintonscott@usgs.gov (C. Scott).
[1] Current address: United States Geological Survey, National Center, Reston, Virginia.

0012-821X/$ – see front matter Published by Elsevier B.V.
http://dx.doi.org/10.1016/j.epsl.2013.12.010

fluctuating surface oxidation state in the Proterozoic undermine the proposed link between late Neoproterozoic oxygenation and the evolution of animals?

The apparent rise and fall in the Earth's oxidation state during the early Paleoproterozoic is coincident with the GOE and the Lomagundi carbon isotope excursion (LCIE), a massive ($\sim+10‰$) and long-lived ($\sim$2200 to 2100 Ma) seawater carbon isotope excursion that is captured in sedimentary carbonates from numerous Paleoproterozoic basins distributed worldwide (Schidlowski et al., 1976; Karhu and Holland, 1996; Bekker et al. 2003a, 2003b). The LCIE has been interpreted as reflecting increased organic carbon burial, which could have released $>20\times$ the amount of oxygen in the present atmospheric reservoir (Karhu and Holland, 1996). This pulse of oxygen must have influenced the chemical composition of seawater.

Because there is a direct, although complicated, relationship between the oxidation state of Earth's surface environments and the concentration of sulfate in seawater, our understanding of Earth's progressive oxygenation has often utilized records of the SSR. Three principal approaches have been used to estimate the size of the Precambrian SSR: the preservation of sulfate evaporites minerals in shallow-marine deposits (e.g., Schröder et al., 2008) or their absence from the record when evidence for other evaporite deposits is preserved (Pope and Grotzinger, 2003), variability in the concentration and isotopic composition of carbonate-associated sulfate (e.g., Kah et al., 2004; Gellatly and Lyons, 2005; Planavsky et al., 2012), and the isotopic composition of sedimentary pyrite sulfur (e.g., Canfield, 1998; Canfield et al., 2010). Since the rock record is incomplete, it is important to investigate each of these sulfur cycle proxies both independently and collectively in order to best describe the evolution of the SSR.

In this paper we present a multi-proxy study of early Paleoproterozoic black shales with a focus on the multiple-sulfur isotope (^{32}S, ^{33}S, and ^{34}S) record of pyrite sulfur. In support of our sulfur isotope data we also present Fe speciation and bulk organic carbon isotope data. These new data provide insight into the size of the SSR in the early Paleoproterozoic oceans during and immediately after the GOE and thus contribute to the developing picture of fluctuating surface redox conditions in the early Paleoproterozoic.

2. Geological setting

2.1. 2200–2100 Myr old Sengoma Argillite Formation, Pretoria Series, Lobatse, Botswana

The Sengoma Argillite Formation (SAF) is up to 700 m thick and is divided into two upward-shallowing sequences by mafic volcanics. Each sequence is composed of carbonaceous and pyritic argillite with siltstones, minor chert, carbonate, and fine-grained, hematite-rich quartz sandstone layers. Argillites often have convoluted bedding and sandstone dikes. It was deposited in the open-marine, epicontinental Transvaal basin in deltaic to offshore environments and experienced greenschist facies metamorphism.

To date, there are no direct geochronologic constraints on the SAF. However, carbonate rocks above and below the SAF have ^{13}C-enriched carbon isotope compositions indicating their deposition during the peak of the Lomagundi Event (Schidlowski et al., 1976). In addition to this chemostratigraphic constraint, the SAF has also been correlated with the Silverton Formation of the Pretoria Group in South Africa (Key, 1983; Bekker et al., 2008). The Pretoria Group, including the Silverton Formation, is unconformably overlain by felsic volcanic rocks of the Rooiberg Group and intruded by the Bushveld Complex, both having an age of 2.05–2.06 Ga (Walraven, 1997; Olsson et al., 2010). The maximum age is constrained by the underlying 2.22 Ga Hekpoort volcanics (Cornell et al., 1996) and a 2316 ± 7 Ma Re–Os isochron pyrite age for the Rooihoogte-lower Timeball Hill formations (Hannah et al., 2004), which are stratigraphically below the Hekpoort volcanics. We therefore infer that the Sengoma Argillite Formation was deposited between 2.2 and 2.1 Ga, during the peak of the Lomagundi carbon isotope excursion. Samples were collected from the drill-hole STRAT 2 collared near Lobatse (Key, 1983) and represent the carbonaceous argillites from the upper sequence.

2.2. 2100–2000 Myr old Zaonega Formation, Ludikovian Series, Karelia, Russia

The Zaonega Formation consists of a 1500-m-thick sequence of basaltic tuffs, siltstones, mudstones, and cherts and is divided into two subformations: a lower, carbonate–argillite subformation (LZ) and an upper, volcano-sedimentary subformation (UZ) in which the bulk of organic-rich rocks are hosted (Medvedev et al., 2001). The Zaonega Formation experienced greenschist facies metamorphism (Melezhik et al., 1999). In the Lake Onega area, the LZ rests disconformably on Upper Jatulian Series carbonates (Tulomozero Formation) that carry high ($>+10‰$) ^{13}C-enrichments typical of the ca. 2.2–2.1 Ga Lomagundi carbon isotope excursion (Karhu and Holland, 1996; Melezhik et al., 1999; Master et al., 2010), while carbonates of the LZ show ^{13}C-enrichments up to $+7.9‰$ (Yudovich et al., 1991; Tikhomirova and Makarikhin, 1993), suggesting that deposition of the UZ black shales occurred during the late stages of the Lomagundi Event. A minimum age for the Zaonega Formation is constrained by 1983 ± 6.5 and 1984 ± 8 Ma U–Pb ages of the Koikary-Svyatnavolok and Pudozhgora dolerite sills (Filippov et al., 2007). These sills are considered to be co-magmatic with sills and mafic volcanics of the Suisar Formation, which directly overlies the Zaonega Formation with an erosional contact allowing significant age difference between these units.

The UZ is subdivided into three units. Unit 1 consists of dark-grey to black volcaniclastic sandstone, siltstone, and mudstone having ubiquitous carbonate seams and lenses and disseminated sulfides. The unit contains three shungite-bearing shale horizons (I–III) varying in thickness from 12 to 35 m. Unit 2 is composed of organic-rich shale, siltstone, dolomite and basaltic lava flows and contains six 5- to 20-m-thick shungite-bearing shale horizons (IV–IX). Unit 3 is composed of shungite-bearing siltstone with dolomite layers. Samples analyzed in this study were selected from two drill cores. C-175 (219.8 m deep) was collared in the Tolvuya syncline near the Tetyugino shungite occurrence, approximately 500 m to the northwest of the FARDEEP drill-holes 12A and 12B (Kump et al., 2011) and capture the Vth to IXth shungite-bearing horizons of the UZ Unit 1. C-5190 (842 m deep) was drilled southwest of Padma, capturing the IIIrd and IVth shungite-bearing horizons of UZ Unit 2, with all samples below 86.9 m belonging to the IIIrd horizon (see supplementary materials for additional details).

3. Analytical methods

3.1. Pyrite sulfur isotope analysis

Powdered shale samples were subjected to Cr-reduction, and liberated H_2S was trapped in a solution of 10% (w/w) zinc acetate (Canfield et al., 1986). ZnS was subsequently converted to Ag_2S with the addition of $\sim$1 mL of 0.2 M $AgNO_3$. Ag_2S was then reacted in a nickel reaction vessel overnight at $\sim250\,^{\circ}C$ in the presence of excess F_2. The resulting SF_6 was purified, first cryogenically and then with a gas chromatograph. Purified SF_6 was introduced to a ThermoFinnigan MAT 253 dual-inlet gas-source isotope-ratio mass-spectrometer where sulfur isotope abundances were measured by monitoring the $^{32}SF^{5+}$, $^{33}SF^{5+}$, $^{34}SF^{5+}$, and $^{36}SF^{5+}$ ion beams at mass to charge ratio of $m/z = 127, 128, 129,$ and 131,

respectively. Isotopic compositions are reported using delta notation:

$$\delta^{3i}S = \left(\frac{^{3i}R_{pyrite}}{^{3i}R_{V\text{-}CDT}} - 1\right) \times 1000,$$

where $^{3i}R = {}^{3i}S/{}^{32}S$, i is 3 or 4, and V-CDT refers to the Vienna-Cañon Diablo Troilite international reference scale. On the V-CDT scale, the $\delta^{34}S$ value of the Ag_2S reference material, IAEA-S-1, is defined as −0.3‰. Capital delta notation is used in order to highlight differences between the fractionation relationships of ^{33}S–^{32}S and ^{34}S–^{32}S ratios:

$$\Delta^{33}S = \delta^{33}S - 1000 \times \left(\left(1 + \frac{\delta^{34}S}{1000}\right)^{0.515} - 1\right).$$

We take the $\Delta^{33}S$ value of IAEA-S-1 to be 0.094‰. The analytical reproducibility (1σ) for the full measurement procedure (extraction, fluorination, and mass spectrometry) is estimated to be better than 0.1‰ for $\delta^{34}S$ values and 0.01‰ for $\Delta^{33}S$ values.

3.2. Organic carbon isotope analysis

The concentration of total organic carbon was determined on an Eltra IR C/S analyzer as the difference between total carbon (determined by combustion) and total inorganic carbon (determined by acidification). For $\delta^{13}C_{org}$ analyses, sample powder was weighed in a silver cup, and ultrapure 6N HCl was added to remove inorganic carbon. In order to improve the efficiency of sample combustion, temperature in the oxidation column was raised to 1100 °C, and a 'macro' O_2 injection loop was utilized. In addition to silver, tin cups were used as a catalyst to increase the reaction temperature through exothermic reaction, ensuring complete combustion. Analyses were performed using a Costech™ 4010 Elemental Analyzer (EA) coupled to a Thermo Finnigan™ Delta V Plus isotope-ratio mass-spectrometer via an open-split interface (ConFlo III, Thermo Finnigan™). All C isotope ratios are reported in delta notation,

$$\delta^{13}C = \left(\frac{^{13}R_{organic\ C}}{^{13}R_{V\text{-}PDB}} - 1\right) \times 1000,$$

relative to international standards on the Vienna-Pee Dee Belemnite (V-PDB) scale. Sample normalization was performed using the two-point calibration described in Coplen et al. (2006). To monitor the quality of sample preparation and analysis performance, the international standard USGS Green River shale SGR-1b ($\delta^{13}C_{org} = -29.3 \pm 0.1$‰ V-PDB) was treated and analyzed as an unknown. Replicate analyses of SGR-1b standard yielded the $\delta^{13}C_{org}$ value of -29.5 ± 0.1‰ ($n = 24$).

3.3. Iron speciation analyses

Iron speciation analyses were performed using a calibrated sequential extraction protocol (Canfield et al., 1986; Poulton and Canfield, 2005) designed to quantify four different pools of highly-reactive iron (Fe_{HR}): (1) pyrite S extracted via Cr-reduction followed by iodometric titration, with Fe calculated assuming an FeS_2 stoichiometry (Fe_{Py}); (2) carbonate-associated iron extracted with a sodium acetate solution (Fe_{Carb}); (3) ferric oxides extracted with a dithionite solution (Fe_{Ox}); and (4) mixed-valence iron oxides, principally magnetite, extracted using ammonium oxalate (Fe_{Mag}). Fe_{Carb}, Fe_{Ox}, and Fe_{Mag} were extracted sequentially using ~100 mg of sample powder, and the sequential extracts were analyzed using an Agilent 7500ce ICP-MS. Based on duplicate analyses, reproducibility of sequentially extracted Fe measurements was better than 95%. We measured bulk Fe and Al concentrations using an Agilent 7500ce ICP-MS following multi-acid (HF–HNO_3–HCl) digestion of powdered and ashed samples (see Scott et al., 2008, for method details).

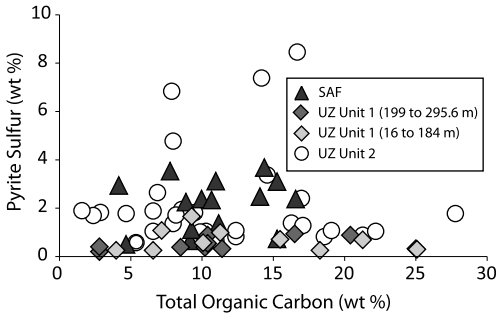

Fig. 1. Pyrite sulfur and total organic carbon concentrations. Sengoma Argillite Formation (triangles), Upper Zaonega, Unit 1 199 to 295.6 m (dark grey diamonds), Upper Zaonega, Unit 2 16 to 184 m (light grey diamonds) and Upper Zaonega Unit 2 (open circles).

4. Results

Both the SAF and UZ shales contain abundant total organic carbon (TOC) and pyrite sulfur (S_{py}), with some UZ enrichments of TOC exceeding 25 wt% (Fig. 1). Pyrite multiple-sulfur isotope data are presented as $\delta^{34}S$ values and $\Delta^{33}S$ values in Fig. 2. Sulfur isotope fractionation associated with dissimilatory sulfate reduction (DSR) can produce $\delta^{33}S$ values that are slightly different than those predicted for thermodynamic equilibrium (Farquhar et al., 2003). The difference can be quantified as $\Delta^{33}S$ values ($= \delta^{33}S_{measured} - \delta^{33}S_{predicted}$), which, in combination with $\delta^{34}S$ values, produce triple-sulfur isotope arrays ($\delta^{34}S$–$\Delta^{33}S$) that provide unique constraint on sulfate supply during DSR (Johnston et al., 2006). $\delta^{34}S$ and $\Delta^{33}S$ values for the analyzed samples cover a wide but systematic range (Fig. 2). All S_{py} from the SAF records negative $\delta^{34}S$ and positive $\Delta^{33}S$ values (Fig. 2a), with increasingly negative $\delta^{34}S$ values coupled to increasingly positive $\Delta^{33}S$ values. Samples from the UZ Unit 1 display a similar inverse relationship between $\delta^{34}S$ and $\Delta^{33}S$ values but also include pyrite with positive $\delta^{34}S$ and negative $\Delta^{33}S$ that converge on values of 15‰ and −0.05‰, respectively (Fig. 2b). For Unit 1, there is a clear stratigraphic division, with samples taken from depths of 199 meters and below displaying negative $\delta^{34}S$ and positive $\Delta^{33}S$ values and samples from 184 meters and above displaying positive $\delta^{34}S$ and negative $\Delta^{33}S$ values. S_{py} from the UZ Unit 2 exhibits uniformly positive $\delta^{34}S$ values (up to 25‰) and both positive and negative $\Delta^{33}S$. For this unit, there is no correlation between the two sulfur isotope parameters and no stratigraphic trend (see supplementary materials, Table S1).

We use Fe speciation analysis to characterize redox conditions in the depositional environment. By convention, when the ratio of highly reactive Fe to total Fe (Fe_{HR}/Fe_T) exceeds 0.4, and the ratio of pyrite Fe to highly reactive Fe (Fe_{PY}/Fe_{HR}) exceeds 0.7, the depositional environment is interpreted to have been euxinic, where bottom waters are both anoxic and contain hydrogen sulfide (Poulton and Canfield, 2011). When Fe_{PY}/Fe_{HR} values are below 0.7 they are interpreted to be oxic, anoxic, or ferruginous (anoxic and Fe-rich). Importantly, sulfide production in non-euxinic environments is restricted to pore waters, below the sediment-water interface, while in euxinic environments sulfide production occurs in both the water column and the shallow sediments. Under this interpretative framework, Fe speciation in samples from the SAF and UZ cores identifies both euxinic and non-euxinic intervals of deposition (Fig. 3). Most samples from the SAF and UZ Unit 2 indicate euxinic deposition, whereas most of the samples from the UZ Unit 1 represent non-euxinic conditions.

The isotopic composition of organic matter in the analyzed samples falls into two clusters that are tightly coupled to the isotopic composition of S_{py} (Fig. 4). Specifically, for samples with $\delta^{34}S$ values <0‰, $\delta^{13}C$ values average ~ −27‰. For samples with $\delta^{34}S$

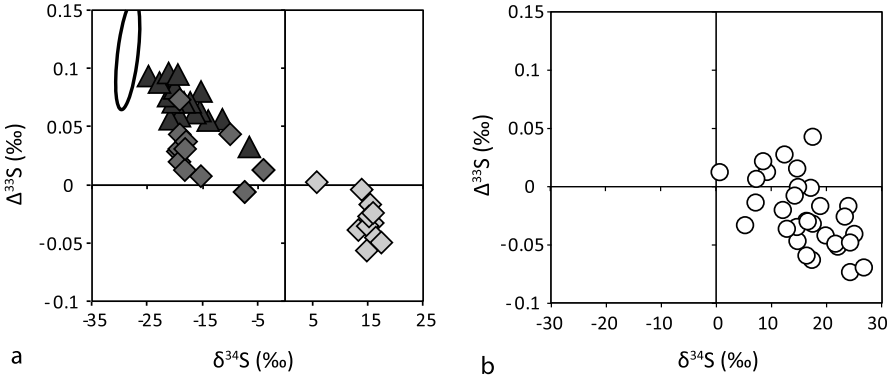

Fig. 2. Pyrite multiple-sulfur isotope data. (a) Sengoma Argillite Formation (triangles) and Upper Zaonega, Unit 1 (199 to 295.6 m dark grey diamonds; 16 to 184 m light grey diamonds) and Upper Zaonega Unit 2 (open circles). Uncertainty ellipse is for the average isotopic composition of nodular pyrite from the 2.32 Ga Rooihoogte and Lower Timeball Hill formations (Bekker et al., 2004), (b) Upper Zaonega, Unit 2.

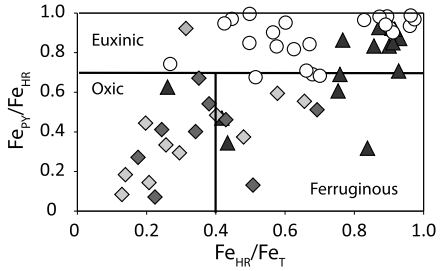

Fig. 3. Fe_{HR}/Fe_T versus Fe_{PY}/Fe_T. Solid lines denote euxinic, oxic, and ferruginous bottom waters fields. Sengoma Argillite Formation (triangles), Upper Zaonega, Unit 1 199 to 295.6 m (dark grey diamonds), Upper Zaonega, Unit 2 16 to 184 m (light grey diamonds) and Upper Zaonega Unit 2 (open circles).

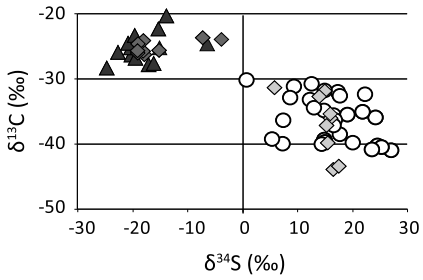

Fig. 4. Organic carbon ($\delta^{13}C$) and pyrite sulfur ($\delta^{34}S$) isotope data. Sengoma Argillite Formation (triangles), Upper Zaonega, Unit 1 199 to 295.6 m (dark grey diamonds), Upper Zaonega, Unit 2 16 to 184 m (light grey diamonds) and Upper Zaonega Unit 2 (open circles).

values $>0‰$, $\delta^{13}C$ values cover a wider range of -30 to $-45‰$, likely reflecting carbon contributed by secondary producers such as methanotrophs and S oxidizers.

5. Discussion

5.1. Pyrite sulfur isotope values, seawater sulfate, and Earth's oxidation state

Since seawater sulfate is derived from oxidative weathering of sulfide minerals on the continents, and the redox state of the oceans controls the S burial flux, seawater sulfate concentrations are tied to the redox state of Earth's atmosphere-ocean system (Canfield, 2005). Furthermore, the isotopic composition of sedimentary pyrites can provide information on the concentration and isotopic composition of seawater sulfate in the local environment and in the open ocean. Thus, the isotopic properties of sedimentary pyrite can be used as a valuable, first-order indicator for the size of the SSR and a rough proxy for the oxidation state of Earth's surface (e.g., Canfield, 1998).

The primary source of sulfide in organic carbon-rich sediments is dissimilatory sulfate reduction (DSR) coupled to oxidation of organic matter, with the resultant hydrogen sulfide sequestered primarily as pyrite (FeS_2). As a result of the enzymatic processes involved in the reduction of sulfate, DSR produces sulfide that is enriched in the light sulfur isotopes relative to precursor sulfate. The upper limit of isotopic fractionation in culture experiments reaches 65‰ for $\delta^{34}S$ values (Sim et al., 2011) and is set by intrinsic metabolic controls (Bradley et al., 2011). However, sulfate uptake also exerts a strong influence on the isotopic composition of the sulfide produced during DSR. The biological sulfur isotope effect will decrease rapidly as sulfate concentration drops to low levels, leading to less reversible sulfate uptake. Previous work demonstrated that below roughly 200 μM sulfide is fractionated by less than ~10‰ relative to the original sulfate (Habicht et al., 2002), although recent work on modern environment suggest that the threshold for reduced fractionation might found at even lower sulfate concentrations (Gomes and Hurtgen, 2013).

Sulfate uptake is not the only biological variable that can influence the magnitude of sulfur isotope fractionations. High rates of cell-specific sulfate reduction result in small isotopic fractionations (Harrison and Thode, 1957; Leavitt et al., 2013) when coupled, for example, to elevated temperatures or supplies of labile organic matter. However, the sulfate reduction rates that produce fractionations <10‰ in pure cultures far exceed the rates observed in natural environments (Hoehler and Jørgensen, 2013), suggesting that this control is not critical in setting the isotopic characteristics of natural samples. Small biological fractionations can also result at low sulfate reduction rates when H_2 is the primary electron donor rather than organic matter (Kaplan and Rittenberg, 1964). Since the samples analyzed in this study contain abundant organic carbon, this mechanism seems unlikely. Thus, we consider sulfate uptake to be the most parsimonious explanation for a biological control of the sulfur isotope fractionations preserved in the organic carbon-rich black shales analyzed in this study.

Transport of sulfur species within sedimentary pore waters can modify how intrinsic biological isotope effects are preserved in sedimentary sulfides (Jørgensen, 1979). Despite the presence of abundant sulfate in overlying seawater, sulfate limitation can develop in sediments where sulfate is consumed faster than it can be replenished by diffusion (Goldhaber and Kaplan, 1975). Here, the isotopic composition of sedimentary sulfide approaches that of seawater sulfate due to limited sulfate supply to the site of sulfate reduction rather than the biological consequences of restricted reversibility of sulfate uptake. For this reason, it is important to distinguish the locus of sulfate reduction when using pyrite sulfur

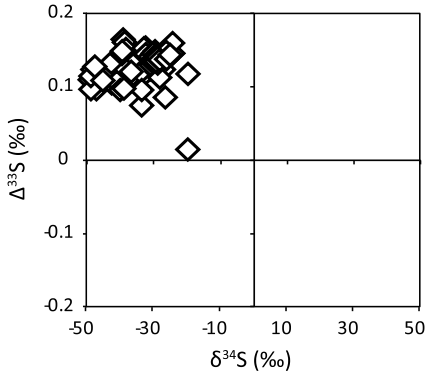

Fig. 5. Pyrite multiple sulfur isotope plots for modern euxinic environments. Data are from the Black Sea (Johnston et al., 2008a, 2008b), Mediterranean sapropels (Scheiderich et al., 2010), Green Lake, New York (Zerkle et al., 2010) and Cariaco basin (Li et al., 2010).

isotopes to estimate the size of the SSR. We address this problem using Fe speciation analysis.

Iron speciation is traditionally used to distinguish between euxinic conditions, where bottom waters are anoxic and sulfidic, and non-euxinic conditions, where bottom waters can be oxic or anoxic, but sulfide is always restricted to pore waters. For this study, we consider euxinic conditions as indicative of open-system sulfate reduction in the water column and the surface sediments (Lyons, 1997; Jørgensen et al., 2001), and non-euxinic conditions as indicative of a more closed system where sulfate reduction is restricted to pore waters. We stress that since highly reactive Fe is unlikely to be transported through a sulfide bearing water column, pyrite formation in euxinic setting occurs dominantly in the water column (e.g., Lyons, 1997). We do not imply that in all cases pore-water sulfate reduction results in sulfate limitation, rather we emphasize that the link between pyrite sulfur isotopes and seawater sulfate concentrations is most straightforward when pyrite forms under euxinic conditions where diffusion of sulfate into the pore waters is less likely to result in sulfate limitation.

For pyrites that formed under euxinic conditions, the following, first-order interpretations hold: (1) $\delta^{34}S$ values that are depleted relative to coeval seawater sulfate by more than 20‰ reflect sulfate-replete conditions (e.g., Lyons, 1997) and therefore generally more oxidized surface environments and (2) $\delta^{34}S$ values approaching those of seawater sulfate reflect sulfate-poor conditions (Habicht et al., 2002) and imply a lower surface oxidation state.

We can expand upon these interpretations and provide unique constraints on sulfate supply by measuring $\delta^{33}S$ values. As described above, fractionation by DSR produces sulfide with $\delta^{33}S$ values that are slightly more positive than those predicted for thermodynamic equilibrium based on $\delta^{34}S$ ratios (Farquhar et al., 2003). Today's oxygen-rich atmosphere supplies marine environments with abundant sulfate (28 mM). With this high capacity for sulfate supply, in combination with bacterially mediated sulfur disproportionation, the resultant sulfide retains positive $\Delta^{33}S$ and highly negative $\delta^{34}S$ values that are characteristic of sulfides produced by DSR under modern conditions (Fig. 5). There are, as of yet, no $\Delta^{33}S$ values published for sedimentary sulfides from modern pore-water environments where sulfate is limiting, but studies of pure cultures suggest that as $\delta^{34}S$ values of sulfide become more positive, $\Delta^{33}S$ values will become less positive due to sulfate limitation (Johnston et al., 2005b).

5.2. The Sengoma Argillite Formation and the rapid expansion of the SSR following the GOE

Our Fe speciation data suggest that the SAF was deposited under predominantly euxinic conditions (Fig. 3) at the peak of the Lomagundi event. The sulfur isotope composition of pyrite in the SAF is characterized by negative $\delta^{34}S$ ratios and positive $\Delta^{33}S$ values (Fig. 2a). The $\delta^{34}S$ values are more than 30‰ lower than $\delta^{34}S$ values estimated for contemporaneous seawater sulfate (+10–14‰; Schröder et al., 2008). This triple S isotope relationship is remarkably similar to that exhibited by recent and modern environments with up to 28 mM seawater sulfate (Fig. 5) and is representative of open system DSR under sulfate-replete conditions. Thus far, microbial S disproportionation is not convincingly evident in the geologic record of S isotopes until the Mesoproterozoic (Johnston et al., 2005a), supporting our interpretation that isotopic composition of SAF pyrite was set by DSR. The precipitation of gypsum before halite in the stratigraphically correlative Lucknow Formation of South Africa requires at least ~2.5 mM sulfate in seawater at that time (Schröder et al., 2008), and the concentration and isotopic composition of contemporaneous carbonate-associated sulfate suggests a minimum seawater sulfate concentration of ~5 mM (Planavsky et al., 2012). Thus, we argue that the isotopic array expressed by the pyrites in the SAF is characteristic of sulfate reduction in the presence of a minimum of 2.5 to 5 mM sulfate.

This concentration range represents a greater than 10-fold increase in the size of the SSR relative to that estimated for the Archean (<200 μM; Habicht et al., 2002; ~80 μM; Jamieson et al., 2012). Nodular pyrites from the ~2320 Ma Rooihoogte and Lower Timeball Hill formations, South Africa, were previously used to calibrate the timing of the GOE (Bekker et al., 2004), and their average $\Delta^{33}S$ and $\delta^{34}S$ values overlap with those from the SAF and modern environments (ellipse in Fig. 2a). Thus, the high seawater sulfate concentrations inferred for the peak of the Lomagundi excursion may have been an immediate response to the GOE and reflectint a rapid accumulation of atmospheric oxygen (*cf.* Bekker and Holland, 2012).

5.3. The Upper Zaonega Subformation and the rapid contraction of the SSR at ~2.05 Ga

It is important to note that the UZ hosts deposits of shungite, amorphous material composed mostly of organic carbon (up to 80 to 98 weight % C_{org}; Melezhik et al., 1999), which have been interpreted as the fossilized remains of migrated bitumen. However, the UZ samples analyzed in this study are not shungite-bearing. While some of these samples contain elevated concentrations of TOC, most of them are indistinguishable from the SAF in terms of their concentrations of TOC, S_{py}, and Al. Furthermore, there is no correlation between the concentration of TOC and the S isotope composition of associated pyrites despite considerable variation in both parameters.

Iron speciation data indicates that pyrite formed in sediment pore waters during deposition of UZ Unit 1 (Fig. 3). There is a broad inverse correlation between $\delta^{34}S$ and $\Delta^{33}S$ values, with data clustered in two stratigraphically defined groups (Fig. 2a) that indicate DSR under different degrees of pore-water sulfate supply (e.g., Johnston et al., 2006). The first group is defined by negative $\delta^{34}S$ and positive $\Delta^{33}S$ values that overlap those of the SAF and occurs stratigraphy lower in the UZ Unit 1 (below 184 m). This group likely reflects sulfate reduction close to the sediment-water interface where sulfate diffusion rates exceeded sulfate reduction rates. The second group is stratigraphically higher (above 184 m) and has positive $\delta^{34}S$ and negative $\Delta^{33}S$ values that cluster tightly around averages of 15‰ and −0.05‰, respectively. Importantly, $\delta^{34}S$ values of the second group approach but do not exceed estimates for contemporaneous seawater sulfate (Planavsky et al., 2012). This clustering of data points is characteristic of a pore-water system where all sulfate entering the diagenetic reaction zone is quantitatively reduced to sulfide and trapped as sedimentary pyrite. In order to maintain such limited variability in pyrite $\Delta^{33}S$ and

δ^{34}S values, the sulfate flux and its isotopic composition must have been relatively constant during deposition of the upper part of UZ Unit. Thus, the second group represents a reasonable estimate of the isotopic composition of seawater sulfate entering the pore waters. The δ^{34}S values of the two groups differ by ~30‰, suggesting that sulfate concentrations in the bottom waters were likely in the mM range throughout deposition of Unit 1, similar to the SAF.

Upper Zaonega Unit 2 captures a subsequent period of euxinic deposition (Fig. 3). However, unlike the euxinic pyrites of the SAF, pyrites in UZ Unit 2 have exclusively positive δ^{34}S values, from ~0 to +25‰, and both positive and negative Δ^{33}S values, from −0.06 to +0.05‰ (Fig. 2b). Within these limits, their isotopic compositions are extremely variable with no discernible stratigraphic trend. We interpret this abrupt transition to highly positive δ^{34}S values in UZ Unit 2, which often exceed the seawater sulfate value inferred from Unit 1, as reflecting an abrupt and substantial contraction in the concentration of seawater sulfate at ~2.05 Ga. In the past, the development of euxinic conditions has been interpreted to reflect relatively sulfate-replete conditions (e.g., Canfield, 1998). However, the identification of euxinic conditions in Archean black shales from the Hamersley Basin in Australia (Reinhard et al., 2009; Scott et al., 2011), demonstrates that euxinic conditions can develop under low sulfate conditions. Thus, our interpretation of a substantial contraction of seawater sulfate in the euxinic UZ Unit 2 basin is not contradictory with the presence of euxinia. We can use Δ^{33}S values to further constrain the magnitude of this contraction.

5.4. *Estimating seawater sulfate concentrations using δ^{34}S and Δ^{33}S values from UZ Unit 2 pyrite*

In order to constrain seawater sulfate concentrations in the euxinic UZ Unit 2 marine environment, we investigated the intrinsic biological fractionation factors that were associated with the δ^{34}S and Δ^{33}S patterns preserved in UZ Unit 2 pyrites. This exercise attempts to answer the following questions:

(1) What is the simplest set of assumptions that is required to reproduce the observed δ^{34}S and Δ^{33}S records?
(2) Are the pyrite δ^{34}S and Δ^{33}S records compatible with the isotopic consequences of water column sulfate limitation?

In a system where sulfate demand by DSR outstrips sulfate supply, sulfate levels will decrease, and residual sulfate will be enriched in the heavy isotopes relative to the starting sulfate (e.g., Gomes and Hurtgen, 2013). Application of isotopic and elemental mass balance to this situation results in a suite of Rayleigh fractionation equations for each ratio of sulfur isotopes in sulfate. For ^{33}S and ^{34}S, these equations are:

$$^{33}R_{sulfate,f} = {}^{33}R_{sulfate,f=1} \times f^{(^{33}\alpha_{pr}-1)}$$
$$^{34}R_{sulfate,f} = {}^{34}R_{sulfate,f=1} \times f^{(^{34}\alpha_{pr}-1)},$$

where f is the fraction of unconsumed sulfate in the local environment and varies between 1 and 0. Taking ^{33}S as an example, $^{33}R_{sulfate,f=1}$ is the ratio of ^{33}S to ^{32}S in the sulfate at the beginning of sulfate consumption ($f = 1$), $^{33}R_{sulfate,f}$ is the ratio of ^{33}S to ^{32}S in the sulfate after consumption has progressed to some value of f less than 1, and $^{33}\alpha_{pr}$ is the fractionation factor describing isotope partitioning between product sulfide (p) and reactant sulfate (s). The fractionation factors are related to each other by:

$$^{33}\alpha_{pr} = \left(^{34}\alpha_{pr}\right)^{^{33}\lambda_{pr}},$$

where $^{33}\lambda_{pr}$ is an exponent that varies systematically with the magnitude of $^{34}\alpha_{pr}$ from ~0.508 to 0.5145 for pure cultures of dissimilatory sulfate-reducing bacteria (Farquhar et al., 2003; Johnston et al., 2005b; Johnston et al., 2007; Sim et al., 2011). There is a positive linear correlation between the magnitude of $^{33}\lambda_{pr}$ and the magnitude of $^{34}\alpha_{pr}$ (expressed as $1000 \times \ln(^{34}\alpha_{pr})$) (Leavitt et al., 2013).

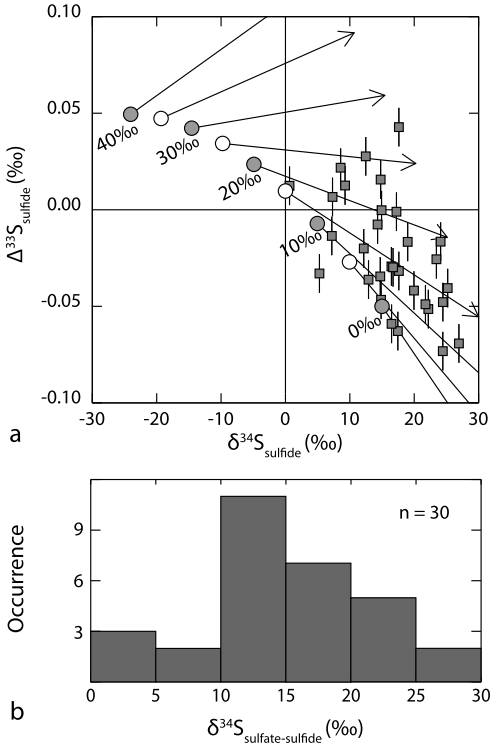

Fig. 6. Predicted Δ^{33}S and δ^{34}S values from Rayleigh model of a sulfate-limited UZ Unit 2 marine environment. (a) White circles are the predicted isotopic compositions of the first-formed sulphide from the initial sulfate pool ($\delta^{34}S = 15‰$, $\Delta^{33}S = -0.05‰$), while arrows are the δ^{34}S and Δ^{33}S trajectories followed by the sulphide produced by DSR under Rayleigh conditions. Grey squares are measured δ^{34}S and Δ^{33}S values from the UZ Unit 2 pyrites; 1σ estimates of the analytical uncertainty in Δ^{33}S values (0.01‰) are shown as thin black lines behind each symbol. Uncertainty in δ^{34}S values (0.1‰) is smaller than the size of the symbols. (b) Histogram of the modeled ^{34}S–^{32}S fractionations associated with DSR in the UZ Unit 2 water column.

With this relationship and the initial sulfate isotope composition inferred from pyrites of the UZ Unit 1 shales ($\delta^{34}S = 15‰$ and $\Delta^{33}S = -0.05‰$), we varied $^{34}\alpha_{pr}$ and predicted (1) the isotopic composition of the first-formed product sulfide in a Rayleigh removal process and (2) the δ^{34}S and Δ^{33}S trajectory taken by the instantaneous sulfide formed in a Rayleigh removal process (Fig. 6a). This produced a graphical framework in which we evaluated the compatibility between our model and the UZ Unit 2 sulfide values.

We counted the number of δ^{34}S and Δ^{33}S pairs from UZ Unit 2 pyrites that fell between each pair of vectors and attributed these measurements to the sub-set of $^{34}\alpha_{pr}$ values that span the two vectors. This exercise reproduced 30 of the 31 measured δ^{34}S and Δ^{33}S pairs in sulfides of the UZ Unit 2 shales. The $^{34}\alpha_{pr}$ values produced by this model correspond to ^{34}S–^{32}S fractionations from near 0‰ to ~27‰ (Fig. 6a). A distinct mode in the set of fractionations occurs between 10‰ and 15‰ (Fig. 6b).

When compared to the experimentally determined relationship between ^{34}S–^{32}S fractionations and sulfate concentrations (see Fig. 2A in Habicht et al., 2002), more than 95% of the modeled ^{34}S–^{32}S fractionations for the UZ Unit 2 are consistent with low sulfate concentrations. Thus, we argue that sustained low sulfate concentrations in the water column are the main biological parameter shaping the paired Δ^{33}S–δ^{34}S data from the Unit 2 shales. Such low sulfate concentrations offer a reasonable explanation for both

the variability in the modeled $^{34}\alpha_{pr}$ values, as well as the apparent Rayleigh behavior of sulfur isotopes in the UZ Unit 2 marine environment. The difference in the inferred sulfate concentrations during the deposition of the UZ Units 1 and 2 can be interpreted as a dramatically fast contraction of the SSR (>10 fold) in the immediate aftermath of the Lomagundi excursion, suggesting a similarly dramatic decrease in the oxidation state of Earth's surface.

5.5. $\delta^{13}C_{org}$ values as indicators of the contraction of the SSR at ~2.05 Ga

Organic carbon $\delta^{13}C$ results from our sample set capture an abrupt negative excursion in the UZ that is coincident with the shift in pyrite S isotope values between Unit 1 and Unit 2 (Fig. 4). A similar negative $\delta^{13}C_{org}$ excursion has been previously reported in the UZ shales (Melezhik et al., 1999; Kump et al., 2011; Qu et al., 2012) and in other correlative successions worldwide (Bekker et al., 2003a, 2003b; Gauthier-Lafaye and Weber, 2003). Kump et al. (2011) interpreted this negative $\delta^{13}C_{org}$ excursion to be global in nature and linked it to oxidation of organic matter on an unprecedented scale, either on the continents or in seawater. Conversely, Qu et al. (2012) linked this excursion to oil and gas generation within the UZ basin, leading to oil and methane seepage onto the seafloor and basinal methanotrophy (which wouldn't be worldwide). Based on the observed C and S isotopic coupling, we propose instead that the excursion reflects a biogeochemical response to the collapse in the marine sulfate reservoir. The low-sulfate conditions postulated here for the UZ Unit 2 should have invigorated biological methane cycling, brought methane production closer to the sediment-water interface, and decreased methane consumption by biologically driven anaerobic oxidation of methane coupled to sulfate reduction. This would allow greater methane fluxes into the overlying water column, where methanotrophy could establish itself at the redoxcline. The observed C isotope depletion in the UZ Unit 2 requires that less than 10% of the total preserved organic carbon was derived from methanotrophy; such proportions are typical of geological environments where methanotrophy is known to be significant (Hayes, 1994). Importantly, laboratory studies demonstrate that methanogens can successfully compete with sulfate reducers when sulfate concentrations fall below 200 μM (e.g., Beal et al., 2011), suggesting that overall methane production is also likely to be enhanced at these low seawater sulfate levels. Thus, the negative coupling of C and S isotopes in the UZ Unit 2 further supports our argument for a collapse to very low concentrations of seawater sulfate at ~2.05 Ga.

5.6. The geologic record of seawater sulfate from ~2.05 to 0.54 Ga

We use our new pyrite multiple-sulfur isotope data to argue for an abrupt shift from sulfate-poor oceans to sulfate-rich oceans as a direct consequence of the initial accumulation of oxygen in the atmosphere at 2.4–2.3 Ga and for an equally abrupt collapse of the SSR at ~2.05 Ga. This scenario is consistent with previous studies describing a rise and fall in the oxidation state of Earth's surface environments (Canfield, 2005; Frei et al., 2009; Bekker and Holland, 2012; Planavsky et al., 2012; Partin et al., 2013). This raises the question of how this apparent crash in seawater sulfate concentrations relates to the SSR during the rest of the Proterozoic Eon.

There are multiple-sulfur isotope data from the ~1.85 Ga Rove Formation, Canada (Poulton et al., 2004), which contains euxinic black shales that were deposited in a foreland basin disconformably above the Gunflint Iron Formation, and from ~1.6–1.4 Ga black shales from the McArthur basin, Australia, that were deposited under oxic and euxinic conditions in open-marine and semi-restricted settings (Shen et al., 2003). With a few exceptions,

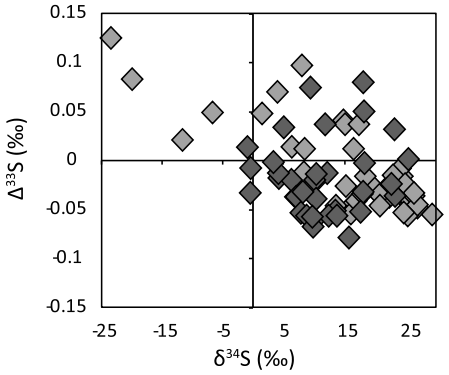

Fig. 7. S isotope data ($\delta^{34}S$ versus $\Delta^{33}S$ values) for the ~1.85 Ga Rove Formation (light-grey diamonds) and the 1.60 to 1.40 Ga McArthur basin shales (dark-grey diamonds). Data are from Johnston et al. (2006, 2008a, 2008b).

these data show positive $\delta^{34}S$ and both positive and negative $\Delta^{33}S$ values (Johnston et al., 2006, 2008a, 2008b), similar to the UZ Unit 2 shales (Fig. 7). In some instances, $\delta^{34}S$ values of pyrite exceed that of coeval seawater sulfate (Johnston et al., 2006). If we further consider the more complete record of traditional $\delta^{34}S$ values from pyrites preserved in black shales (Fig. 8), we find that highly negative $\delta^{34}S$ values are common between ~2.32 and 2.05 Ga, while positive $\delta^{34}S$ values characterize the remainder of the Proterozoic Eon. In general, the depleted $\delta^{34}S$ values that characterize early Paleoproterozoic pyrites ($\delta^{34}S_{sulfate}-\delta^{34}S_{pyrite} > 30‰$) are not observed in euxinic black shales until ~635 Ma (Sahoo et al., 2012), roughly coincident with the first appearance of macroscopic putative metazoans. Taken as a whole, the pyrite sulfur isotope record suggests that the sulfate-replete oceans that characterized the early Paleoproterozoic did not return until the late Neoproterozoic. Estimated sulfate concentrations for the McArthur basin are 2–5 mM (Shen et al., 2002), which provide maximum limits for the Mesoproterozoic and minimum limits for the early Paleoproterozoic. Thus, the late Paleoproterozoic seawater sulfate concentrations probably increased after 2.0 Ga but did not return to early Paleoproterozoic levels until much later.

This scenario is consistent with other records of the Proterozoic SSR. The lack of sulfate minerals in evaporites from the ~1.9 Ga Stark Formation, Northwestern Canada, is taken as evidence for very low seawater sulfate concentrations (Pope and Grotzinger, 2003). Although pseudomorphs replacing sulfate crystals have been reported from younger Paleoproterozoic and Mesoproterozoic successions (e.g., 1.7–1.6 Ga sabkha deposits of the McArthur basin; Walker et al., 1977; McClay and Carlile, 1978), but these are rare and never formed massive beds. The first occurrence of massive beds of gypsum, after those of the early Paleoproterozoic (e.g., Bekker et al., 2003a, 2003b; Schröder et al., 2008; Bekker and Holland, 2012), is in the ca. 1.2 Ga Society Cliff Formation, Borden basin, Canadian Arctic (Jackson and Ianelli, 1981; Kah et al., 2001; Turner, 2004). However, even these beds are stratigraphically minor (5 to 20% locally) and commonly less than 1.5 m thick, with the maximum thickness of 3 m (Jackson and Ianelli, 1981; Turner, 2009). Deposition of globally significant sulfate evaporites did not occur again until the early Neoproterozoic, when shallow-marine sedimentary successions found in the MacKenzie Mountains and Victoria Island, NWT, Canada, and the Amadeus basin, central Australia, contain multiple thick (>100 m) massive beds of sulfate evaporites deposited between 830 and 715 Ma (Young, 1981; Young and Long, 1977; Lindsay, 1987). The terminal Neoproterozoic is also marked by deposition of sulfate evaporites (Schröder et al., 2003).

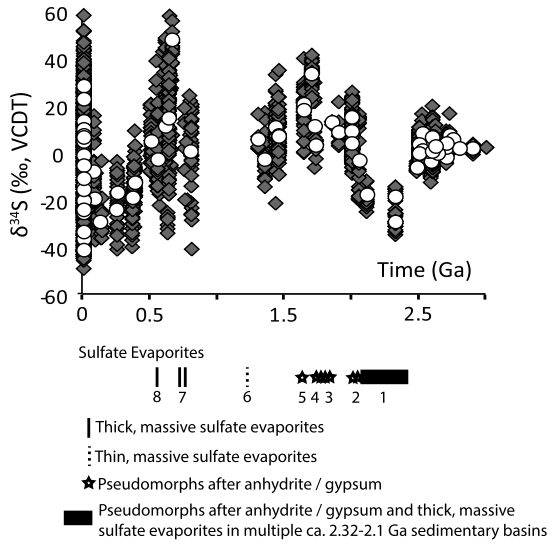

Fig. 8. Comparison of $\delta^{34}S$ values for pyrites in black shales through time and Proterozoic sulfate evaporites. Pyrite timeline modified from Canfield and Farquhar (2009) to include only data for black shales. White circles are average values per unit. Secular distribution of sulfate evaporites in the Proterozoic after Pope and Grotzinger (2003) and Schröder et al. (2008) unless otherwise indicated. Thick, massive sulfate evaporites and extensively developed pseudomorphs after anhydrite/gypsum occur in a number of ca. 2.32–2.1 Ga sedimentary basins on different cratons (1). Pseudomorphs after anhydrite/gypsum (2) are also developed in the ca. 2.0 Ga Kasegalik and McLeary formations of the Belchers Islands and in the 2.0 Ga Coomalie and Celia dolomites of the Pine Creek Orogen (Crick and Muir, 1980). Pseudomorphs after anhydrite/gypsum (3) are common in a number of the 1.9–1.85 Ga sedimentary basins (see Pope and Grotzinger, 2003), including the Tavani Formation of the Hurwitz basin (Aspler et al., 1994) and the Koolpin and Cahill formations of the Pine Creek Orogen (Crick and Muir, 1980). The Corella Formation of the Mount Isa basin (4) is the single known evaporite deposit with pseudomorphs after anhydrite and gypsum of ca. 1.75 Ga age. Pseudomorphs after gypsum and anhydrite (5) are common in several units of the 1.67–1.64 Ga McArthur and Mt Isa groups. Subsequently, evidence for sulfate evaporites reappears only in the ca. 1.2 Ga sedimentary successions of the Borden and Grenville (Whelan et al., 1990) basins (6), where thin, massive sulfate evaporite beds are present. After another long time gap, thick, massive sulfate evaporites (7) emerge in the ca. 830–715 Ma sedimentary successions and bracket the Bitter Spring anomaly in Canada, Australia, and Central Africa. Finally, thick, massive sulfate evaporites (8) became again abundant at the Precambrian–Cambrian boundary in several sedimentary basins in Asia and Australia. Although not indicated here, sulfate evaporites have been buried continuously throughout the Phanerozoic, with variability imposed by variations in submerged continental crust and sea level rather than ocean–atmosphere oxygenation (Halevy et al., 2012).

5.7. Implications for the oxygenation of Earth's surface environments

Although the mechanistic link between Earth's oxidation state and the size of the SSR is complicated, they appear to be positively correlated on geological timescales (Canfield, 2005). Based on the confluence of multiple lines of evidence, including the new multiple S-isotope data reported here, we argue that the size of the SSR between 2.3 and 2.05 Ga was larger than at any point between 2.0 Ga and 635 Ma (Sahoo et al., 2012). As the rise of the SSR in the early Paleoproterozic coincided roughly with the Great Oxidation Event and initiation of the Lomagundi carbon isotope excursion, while the contraction of the SSR is associated with the termination of the Lomagundi event, there appears to be direct relationships among first-order variations in atmospheric oxygen, ocean redox state, and the size of the SSR. Highly ^{34}S-depleted pyrites returned in the Ediacaran Era (Fig. 8) when atmosphere and ocean oxygenation reached levels sufficient for aerobic respiration (Sahoo et al., 2012). Considering the unique similarity between pyrite S isotopes in the SAF and Ediacaran black shales, it seems possible that the concentration of atmospheric oxygen during the Lomagundi carbon isotope excursion approached that of the Ediacaran Era.

Acknowledgements

We thank David Johnston and an anonymous reviewer for providing thoughtful reviews. C.T.S. and B.A.W. acknowledge support from NSERC through a Discovery grant and the CREATE Canadian Astrobiology Training program. The Stable Isotope Laboratory at McGill is supported by FQRNT through the GEOTOP research center. A.B. acknowledges support from NSF grant EAR-05-45484, NASA Astrobiology Institute Award NNA04CC09A, and an NSERC Discovery Grant. The NASA Exobiology Program and the U.S. National Science Foundation provided support to T.W.L. and N.J.P.

Appendix A. Supplementary material

Supplementary material related to this article can be found online at http://dx.doi.org/10.1016/j.epsl.2013.12.010.

References

Aspler, L.B., Chiarenzelli, J.R., Ozarkno, D.L., Powis, K.B., 1994. Geology of Archean and Proterozoic supracrustal rocks in the Otter and Ducker Lakes area, southern District of Keewatin, Northwest Territories. Curr. Res., Geol. Surv. Can. 1994-C, 165–174.

Beal, E.J., Claire, M.W., House, C.H., 2011. High rates of anaerobic methanotrophy at low sulfate concentrations with implications for past and present methane levels. Geobiology 9, 131.

Bekker, A., Holland, H.D., 2012. Oxygen overshoot and recovery during the early Paleoproterozoic. Earth Planet. Sci. Lett. 317–318, 295–304.

Bekker, A., Karhu, J.A., Eriksson, K.A., Kaufman, A.J., 2003a. Chemostratigraphy of Paleoproterozoic carbonate successions of the Wyoming Craton: tectonic forcing of biogeochemical change?. Precambrian Res. 120, 279–325.

Bekker, A., Sial, A.N., Karhu, J.A., Ferreira, V.P., Noce, C.M., Kaufman, A.J., Romano, A.W., Pimentel, M.M., 2003b. Chemostratigraphy of carbonates from the Minas Supergroup, Quadrilatero Ferryifero (Iron Quadrangle), Brazil: A stratigraphic record of early Paleoproterozoic atmospheric, biogeochemical and climatic change. Am. J. Sci. 303, 865–904.

Bekker, A., Holland, H.D., Wang, P.-L., Rumble III, D., Stein, H.J., Hannah, J.L., Coetzee, L.L., Beukes, N.J., 2004. Dating the rise of atmospheric oxygen. Nature 427, 117–120.

Bekker, A., Holmden, C., Beukes, N.J., Kenig, F., Eglington, B., Patterson, W.P., 2008. Fractionation between inorganic and organic carbon during the Lomagundi (2.22–2.1 Ga) carbon isotope excursion. Earth Planet. Sci. Lett. 271, 278–291.

Bradley, A.S., Leavitt, W.D., Johnston, D.T., 2011. Revisiting the dissimilatory sulfate reduction pathway. Geobiology 9, 446–457.

Canfield, D.E., 1998. A new model for Proterozoic ocean chemistry. Nature 396, 450–453.

Canfield, D.E., 2005. The early history of atmospheric oxygen. Annu. Rev. Earth Planet. Sci. 33, 1–36.

Canfield, D.E., Farquhar, J., 2009. Animal evolution, bioturbation and the sulfate concentration of the oceans. Proc. Natl. Acad. Sci. 106, 8123–8127.

Canfield, D.E., Raiswell, R., Westrich, J.T., Reaves, C.M., Berner, R.A., 1986. The use of chromium reduction in the analysis of reduced inorganic sulfur in sediments and shales. Chem. Geol. 54, 149–155.

Canfield, D.E., Farquhar, J., Zerkle, A.L., 2010. High isotope fractionations during sulfate reduction in a low-sulfate euxinic ocean analogue. Geology 38, 415–418.

Coplen, T.B., Brand, W.A., Gehre, M., Gröning, M., Meijer, H.A.J., Toman, B., Verkouteren, R.M., 2006. New guidelines for $\delta^{13}C$ measurements. Anal. Chem. 79, 2439–2441.

Cornell, D.H., Schütte, S.S., Eglington, B.L., 1996. The Ongeluk basaltic andesite formation in Griqualand West, South Africa: submarine alteration in a 2222 Ma Proterozoic sea. Precambrian Res. 79, 101–123.

Crick, I.H., Muir, M.D., 1980. Evaporites and uranium mineralization in the Pine Creek Geosyncline. In: Proceedings of International Uranium Symposium on the Pine Creek Geosyncline, pp. 531–542.

Farquhar, J., Johnston, D.T., Wing, B.A., Habicht, K.S., Canfield, D.E., Airieau, S., Thiemens, M.H., 2003. Multiple sulfur isotopic interpretations of biosynthetic pathways: implications for biological signatures in the sulfur isotope record. Geobiology 1, 27–36.

Filippov, N.B., Melezhik, V.A. (Eds.), 2006. Atlas of Structures and Textures of the Shungite-Bearing Rocks in the Onegian Synclinore. Scandinavia, Petrozavodsk, 80 pp.

Filippov, N.B., Trofimov, N.N., Golubev, A.I., Sergeev, S.A., Huhma, H., 2007. Isotopic age data on the Koikary-Svyatnavolok and Pudozhgora sheeted intrusions. Geol. Useful Miner. Karelia 10, 49–68.

Frei, R., Gaucher, C., Poulton, S.W., Canfield, D.E., 2009. Fluctuations in Precambrian atmospheric oxygenation recorded in chromium isotopes. Nature 461, 250–253.

Gauthier-Lafaye, F., Weber, F., 2003. Natural nuclear fission reactors: time constraints for occurrence, and their relation to uranium and manganese deposits and to the evolution of the atmosphere. Precambrian Res. 120, 81–100.
Gellatly, A.M., Lyons, T.W., 2005. Trace sulfate in mid-Proterozoic carbonates and the sulfur isotope record of biospheric evolution. Geochim. Cosmochim. Acta 69, 3813–3829.
Goldblatt, C., Lenton, T.M., Watson, A.J., 2006. Bistability of atmospheric oxygen and the Great Oxidation. Nature 443, 683–686.
Goldhaber, M.B., Kaplan, I.R., 1975. Controls and consequences of sulfate reduction rates in recent marine sediments. Soil Sci. 119, 42–55.
Gomes, M.L., Hurtgen, M.T., 2013. Sulfur isotope systematics of a euxinic, low-sulfate lake: evaluating the importance of the reservoir effect in modern and ancient oceans. Geology 41, 663–666.
Habicht, K.S., Gade, M., Thamdrup, B., Berg, P., Canfield, D.E., 2002. Calibration of sulfate levels in the Archean ocean. Science 298, 2372–2374.
Halevy, I., Peters, S.E., Fischer, W.W., 2012. Sulfate burial constraints on the Phanerozoic sulfur cycle. Science 337, 331–334.
Hannah, J.L., Bekker, A., Stein, H.J., Markey, R.J., Holland, H.D., 2004. Primitive Os and 2316 Ma age for marine shale: implications for Paleoproterozoic glacial events and the rise of atmospheric oxygen. Earth Planet. Sci. Lett. 225, 43–52.
Harrison, A.G., Thode, H.G., 1957. The isotope effect in the chemical reduction of sulfate. Trans. Faraday Soc. 53, 1648–1651.
Hayes, J.M., 1994. Global methanotrophy at the Archean–Proterozoic transition. In: Bengston, S. (Ed.), Proc. Nobel Symp. 84, Early Life on Earth. Columbia University Press, New York, pp. 220–236.
Hoehler, T.M., Jørgensen, B.B., 2013. Microbial life under extreme energy limitation. Nat. Rev. Microbiol. 11, 83–94.
Holland, H.D., 2002. Volcanic gases, black smokers, and the Great Oxidation Event. Geochim. Cosmochim. Acta 66, 3811–3826.
Jackson, G.D., Ianelli, T.R., 1981. Rift-related cyclic sedimentation in the Neohelikian Borden Basin, northern Baffin Island. In: Campbell, F.H.A. (Ed.), Proterozoic Basins of Canada. Geol. Surv. Can. Paper 81-10, 269–302.
Jamieson, J.W., Wing, B.A., Farquhar, J., Hannington, M.H., 2012. Neoarchean seawater sulphate concentrations from sulphur isotopes in massive sulphide ore. Nat. Geosci. 6, 61–64.
Johnston, D.T., Wing, B.A., Farquhar, J., Kaufman, A.J., Strauss, H., Lyons, T.W., Kah, L.C., Canfield, D.E., 2005a. Active microbial sulfur disproportionation in the Mesoproterozoic. Science 310, 1477–1479.
Johnston, D.T., Farquhar, J., Wing, B.A., Kaufman, A.J., Canfield, D.E., Habicht, K.S., 2005b. Multiple sulfur isotope fractionations in biological systems: a case study with sulfate reducers and sulfur disproportionators. Am. J. Sci. 305, 645–660.
Johnston, D.T., Poulton, S.W., Fralick, P.W., Wing, B.A., Canfield, D.E., Farquhar, J., 2006. Evolution of the sulfur cycle at the end of the Paleoproterozoic. Geochim. Cosmochim. Acta 70, 5723–5739.
Johnston, D.T., Farquhar, J., Canfield, D.E., 2007. Sulfur isotope insights into microbial sulfate reduction: when microbes meet models. Geochim. Cosmochim. Acta 71, 3929–3947.
Johnston, D.T., Farquhar, J., Summons, R.E., Shen, Y., Kaufman, A.J., Masterson, A.L., Canfield, D.E., 2008a. Sulfur isotope biogeochemistry of the Proterozoic McArthur Basin. Geochim. Cosmochim. Acta 72, 4278–4290.
Johnston, D.T., Farquhar, J., Habicht, K.S., Canfield, D.E., 2008b. Sulphur isotopes and the search for life: strategies for identifying sulphur metabolisms in the rock record and beyond. Geobiology 6, 425–435.
Jørgensen, B.B., 1979. A theoretical model of the stable sulfur isotope distribution in marine sediments. Geochim. Cosmochim. Acta 43, 363–374.
Jørgensen, B.B., Weber, A., Zopfi, J., 2001. Sulfate reduction and anaerobic methane oxidation in Black Sea sediments. Deep-Sea Res. I 48, 2097–2120.
Kah, L.C., Lyons, T.W., Chesley, J.T., 2001. Geochemistry of a 1.2 Ga carbonate-evaporites succession, northern Baffin Island: implications for Mesoproterozoic marine evolution. Precambrian Res. 111, 203–234.
Kah, L.C., Lyons, T.W., Frank, T.D., 2004. Low marine sulphate and protracted oxygenation of the Proterozoic biosphere. Nature 431, 834–838.
Kaplan, I.R., Rittenberg, S.C., 1964. Carbon isotope fractionation during metabolism of lactate by Desulfovibrio desulfuricans. J. Gen. Microbiol. 34, 213–217.
Karhu, J.A., Holland, H.D., 1996. Carbon isotopes and the rise of atmospheric oxygen. Geology 24, 867–870.
Key, R.M., 1983. The Geology of the Area Around Gaborone and Lobatse Kweneng, Kgatleng, Southern and South East Districts Gaborone. Geol. Surv. Botswana, District Mem., vol. 5, p. 230.
Kump, L.R., Junium, C., Arthur, M.A., Brasier, A., Fallick, A., Melezhik, V., Lepland, A., Črne, A.E., Luo, G., 2011. Isotopic evidence for massive oxidation of organic matter following the Great Oxidation Event. Science 334, 1694–1696.
Leavitt, W.D., Halevy, I., Bradley, A.S., Johnston, D.T., 2013. Influence of sulfate reduction rates on the Phanerozoic sulfur isotope record. Proc. Natl. Acad. Sci. 110, 11244–11249.
Li, X., Gilhooly, W.P., Zerkle, A.L., Lyons, T.W., Farquhar, J., Werne, J.P., Varela, R., Scranton, M.I., 2010. Stable sulfur isotopes in the water column of the Cariaco Basin. Geochim. Cosmochim. Acta 74, 6764–6778.
Lindsay, J.F., 1987. Upper Proterozoic evaporites in the Amadeus basin, central Australia, and their role in basin tectonics. Geol. Soc. Am. 99, 852–865.
Lyons, T.W., 1997. Sulfur isotopic trends and pathways of iron sulfide formation in upper Holocene sediments of the Black Sea. Geochim. Cosmochim. Acta 61, 3367–3382.
Master, S., Bekker, A., Hofmann, A., 2010. A review of the stratigraphy and geological setting of the Palaeoproterozoic Magondi Supergroup, Zimbabwe – Type locality for the Lomagundi carbon isotope excursion. Precambrian Res. 182, 254–273.
McClay, K.R., Carlile, D.G., 1978. Mid-proterozoic sulphate evaporites at Mount Isa mine, Queensland, Australia. Nature 274, 240–241.
Medvedev, P.V., Philippov, M., Romashkin, A.E., Vavra, N., 2001. Primary organic matter and lithofacies of siliceous shungite rocks from Karelia. Neues Jahrb. Geol. Paläontol. Abh. 11, 641–658.
Melezhik, V.A., Fallick, A.E., Filippov, M.M., Larsen, O., 1999. Extreme $^{13}C_{carb}$ enrichment in ca. 2.0 Ga magnesite-stromatolite-dolomite 'red beds' association in a global context: a case for the world-wide signal enhanced by a local environment. Earth-Sci. Rev. 1, 71–120.
Narbonne, G.M., 2005. The Ediacaran biotoa: Neoproterozoic origin of animals and their ecosystems. Annu. Rev. Earth Planet. Sci. 33, 421–442.
Olsson, J.R., Söderlund, U., Klausen, M.B., Ernst, R.E., 2010. U–Pb baddeleyite ages linking major Archean dyke swarms to volcanic-rift forming events in the Kaapvaal craton (South Africa), and a precise age for the Bushveld Complex. Precambrian Res. 183, 490–500.
Ozaki, K., Tajika, E., 2013. Biogeochemical effects of atmospheric oxygen concentration, phosphorus weathering, and sea-level stand on oceanic redox chemistry: Implications for greenhouse climates. Earth Planet. Sci. Lett. 373, 129–139.
Partin, C.A., Bekker, A., Planavsky, N.J., Scott, C.T., Bill, B.C., Li, C., Podkovyrov, V., Maslov, A., Konhauser, K.O., Lalonde, S.V., Love, G.D., Poulton, S.W., Lyons, T.W., 2013. Large-scale fluctuations in Precambrian atmospheric and oceanic oxygen levels from the record of U in shales. Earth Planet. Sci. Lett. 369–370, 284–293.
Pavlov, A.A., Kasting, J.F., 2002. Mass-independent fractionation of sulfur isotopes in Archean sediments: strong evidence for an anoxic Archean atmosphere. Astrobiology 2, 27–41.
Planavsky, N.J., Bekker, A., Hofmann, A., Owens, J.D., Lyons, T.W., 2012. Sulfur record of rising and falling marine oxygen and sulfate levels during the Lomagundi event. Proc. Natl. Acad. Sci. 109, 18300–18305.
Pope, M.C., Grotzinger, J.P., 2003. Paleoproterozoic Stark Formation, Athapuscow Basin, Northwest Canada: record of cratonic-scale salinity crisis. J. Sediment. Res. 73, 280–295.
Poulton, S.W., Canfield, D.E., 2005. Development of a sequential extraction procedure for iron: implications for iron partitioning in continentally derived particulates. Chem. Geol. 214, 209–221.
Poulton, S.W., Canfield, D.E., 2011. Ferruginous conditions: a dominant feature of the ocean though Earth's history. Elements 7, 107–112.
Poulton, S.W., Fralick, P.W., Canfield, D.E., 2004. The transition to a sulphidic ocean similar to 1.84 billion years ago. Nature 431, 173–177.
Qu, Y., Črne, A.E., Lepland, A., van Zuilen, M.A., 2012. Methanotrophy in a Paleoproterozoic oil field ecosystem, Zaonega Formation, Karelia, Russia. Geobiology 10, 467–478.
Reinhard, C.T., Raiswell, R., Scott, C.T., Anbar, A.D., Lyons, T.W., 2009. A late Archean sulfidic sea stimulated by early oxidative weathering of the continents. Science 326, 713–716.
Sahoo, S.K., Planavsky, N.J., Kendall, B., Wang, X., Shi, X., Scott, C., Anbar, A.D., Lyons, T.W., Jiang, G., 2012. Ocean oxygenation in the wake of the Marinoan glaciation. Nature 498, 546–549.
Scheiderich, K., Zerkle, A.Z., Helz, G.R., Farquhar, J., Walker, R.J., 2010. Molybdenum isotope, multiple sulfur isotope, and redox-sensitive element behavior in early Pleistocene Mediterranean sapropels. Chem. Geol. 279, 134–144.
Schidlowski, M., Eichmann, R., Junge, C.E., 1976. Carbon isotope geochemistry of the Precambrian Lomagundi carbonate province, Rhodesia. Geochim. Cosmochim. Acta 40, 449–455.
Schröder, S., Schreiber, B.C., Amthor, J.E., Matter, A., 2003. A depositional model for the terminal Neoproterozoic-Early Cambrian Ara Group evaporites in south Oman. Sedimentology 50, 879–898.
Schröder, S., Bekker, A., Beukes, N.J., Strauss, H., van Niekerk, H.S., 2008. Rise in seawater sulphate concentration associated with the Paleoproterozoic positive carbon isotope excursion: evidence from sulphate evaporites in the 2.2–2.1 Gyr shallow marine Lucknow Formation, South Africa. Terra Nova 28, 108–117.
Scott, C., Lyons, T.W., Bekker, A., Shen, Y., Poulton, S., Chu, X., Anbar, A., 2008. Tracing the stepwise oxygenation of the Proterozoic biosphere. Nature 452, 456–459.
Scott, C., Bekker, A., Reinhard, C.T., Schnetger, B., Krapež, B., Rumble III, D., Lyons, T.W., 2011. Late Archean euxinic conditions before the rise of atmospheric oxygen. Geology 39, 119–122.
Shen, Y., Canfield, D.E., Knoll, A.H., 2002. Middle Proterozoic ocean chemistry: evidence from McArthur Basin, Northern Australia. Am. J. Sci. 302, 81–109.
Shen, Y., Knoll, A.H., Walter, M.R., 2003. Evidence for low sulfate and anoxia in a mid-Proterozoic marine basin. Nature 423, 632–635.
Sim, M.S., Bosak, T., Ono, S., 2011. Large sulfur isotope fractionation does not require disproportionation. Science 333, 74–77.
Tikhomirova, M., Makarikhin, V.V., 1993. Possible reasons for the $\delta^{13}C$ anomaly of Lower Proterozoic sedimentary carbonates. Terra Nova 5, 244–248.

Turner, E.C., 2004. Origin of basinal carbonate laminites of the Mesoproterozoic Society Cliffs Formation (Borden Basin, Nunavut), and implications for base-metal mineralization. Curr. Res., Geol. Surv. Can. 2004-B2. 12 pp.

Turner, E.C., 2009. Mesoproterozoic carbonate systems in the Borden basin, Nunavut. Can. J. Earth Sci. 46, 915–938.

Walker, R.N., Muir, M.D., Diver, W.L., Williams, N., Wilkins, N., 1977. Evidence of major sulphate evaporite deposits in the Proterozoic McArthur Group, Northern Territory, Australia. Nature 265, 526–529.

Walraven, F., 1997. Geochronology of the Rooiberg Group, Transvaal Supergroup, South Africa, Johannesburg, South Africa, Econ. Geol. Res. Unit, University of the Witwatersrand. Info Circuits 316. 21 pp.

Whelan, J.F., Rye, R.O., deLorraine, W., Ohmoto, H., 1990. Isotopic geochemistry of a Mid-Proterozoic evaporite basin. Am. J. Sci. 290, 396–424.

Young, G.M., 1981. The Anundsen embayment, Northwest Territories: Relevance to the Upper Proterozoic Evolution of North America. In: Campbell, F.H.A. (Ed.), Proterozoic Basins of Canada. Geol. Surv. Can. Paper 81-10, 203–218.

Young, G.M., Long, D.G.E., 1977. Carbonate sedimentation in a late Precambrian shelf sea, Victoria Island, Canadian Arctic Archipelago. J. Sediment. Res. 47, 943–955.

Yudovich, Y.Y., Makarikhin, V.V., Medvedev, P.V., Sukhanov, N.V., 1991. Carbon isotope anomalies in carbonates of the Karelian Complex. Geochem. Intern. 28, 56–62.

Zerkle, A.L., Kamyshny Jr., A., Kump, L.R., Farquhar, J., Oduro, H., Arthur, M.A., 2010. Sulfur cycling in a stratified euxinic lake with moderately high sulfate: constraints from quadruple sulfur isotopes. Geochim. Cosmochim. Acta 74, 4953–4970.